

# Surpassing the standard quantum limit in an atom interferometer with four-mode entanglement produced from four-wave mixing

S. A. Haine<sup>1,\*</sup> and A. J. Ferris<sup>2</sup><sup>1</sup>*Australian Research Council Centre of Excellence for Quantum-Atom Optics, University of Queensland, Brisbane, 4072, Australia*<sup>2</sup>*University of Sherbrooke, Canada*

(Received 5 August 2011; published 14 October 2011)

We theoretically investigate a scheme for atom interferometry that surpasses the standard quantum limit. A four-wave mixing scheme similar to the recent experiment performed by Pertot *et al.* [*Phys. Rev. Lett.* **104**, 200402 (2010)] is used to generate subshotnoise correlations between two modes. These two modes are then interfered with the remaining two modes in such a way as to surpass the standard quantum limit, whilst utilizing all of the available atoms. Our scheme can be viewed as using two correlated interferometers. That is, the signal from each interferometer when looked at individually is classical, but there are correlations between the two interferometers that allow for the standard quantum limit to be surpassed.

DOI: [10.1103/PhysRevA.84.043624](https://doi.org/10.1103/PhysRevA.84.043624)

PACS number(s): 37.25.+k, 67.85.Fg

## I. INTRODUCTION

Atom interferometry [1] is a useful tool for sensitive measurements of gravitational fields and accelerations [2,3], gravitational gradients [4], rotations [5], magnetic fields [6], the gravitational constant ( $G$ ) [7], and the fine structure constant ( $\alpha$ ) [8]. Although most state-of-the-art atom interferometers currently utilize laser cooled atoms, there may be some benefit to using Bose-Einstein-condensed atoms. Bose-Einstein-condensed atoms provide improved visibility in configurations which require complex manipulation of the motional state, such as high-momentum-transfer beam splitters [9]. The ultimate limit of the sensitivity of any interferometric device which uses uncorrelated particles in each arm is the standard quantum limit  $\Delta\phi = \frac{1}{\sqrt{N_t}}$ , where  $N_t$  is the total number of detected particles [10].

Recently, there has been much interest in surpassing this limit in atom interferometers via the use of quantum entanglement, with two recent proof-of-principles experiments demonstrating subshotnoise phase sensing [11,12]. These experiments exploit the  $s$ -wave scattering to provide one-axis twisting [13,14] to generate spin squeezing in the two atomic modes. However, both of these experiments use only a small number of atoms (200–1200 atoms), so the absolute sensitivity of the device is low. It is unlikely that the number of atoms used in this scheme can be increased significantly, as the phase correlations produced become very sensitive to classical uncertainty in the total number of particles as the total number of particles is increased.

Atomic four-wave mixing [15] has long been considered a possible method of creating entanglement between spatially separated atomic modes [16–23], and the generation and detection of quantum correlations using this process has recently been demonstrated [24,25]. Four-wave mixing has an advantage over one-axis-twisting schemes because the correlations produced by the interaction are number correlations and are not as sensitive to the total number of particles. However,

it is so far unclear how best to utilize these correlations for the purpose of atom interferometry. We consider a setup similar to the recent experiment of Pertot *et al.* [26]. Here, collisions between two electronic states allow for collinear four-wave mixing, which can be well represented by a four-mode model. A simple theory predicts that the two modes with low occupation number display subshotnoise quantum correlations. However, in order to increase the sensitivity of our device, we devise an interferometry scheme which utilizes *all* of the available atoms, such that it is possible to surpass the standard quantum limit while retaining a larger number of atoms.

The structure of this paper is as follows: In Sec. II, we describe our proposed scheme. In Sec. III, we introduce a simple four-mode model to calculate the level of quantum correlations generated from the four-wave mixing process. In Sec. IV we introduce a more realistic multimode model that allows for effects such as spatial inhomogeneity and multiple-order scattering. In Sec. V we demonstrate how this system can be used to perform an interferometric phase measurement which surpasses the standard quantum limit and, in Sec. VI, we compare our scheme to one-axis twisting for a large number of particles.

## II. FOUR-WAVE MIXING

Our scheme involves two stages: The state preparation stage (Fig. 1) and the interferometry stage. We begin the state preparation stage with a Bose-Einstein condensate (BEC) containing approximately  $2 \times 10^5$  <sup>87</sup>Rb atoms, tightly confined in the  $z$  and  $y$  direction and weakly confined in the  $x$  direction. The  $x$  confinement is switched off before the state preparation begins. All atoms are in the  $|a\rangle \equiv |F=1, m_F=1\rangle$  hyperfine state. To induce the four-wave mixing, we couple approximately 50% of the atoms to the  $|b\rangle \equiv |F=2, m_F=0\rangle$  hyperfine state via a two-photon Raman transition, which also transfers linear momentum  $\hbar k_0$  to the atoms. In addition, we use resonant microwave coupling to transfer a small amount of population (approximately 1%) between  $|a\rangle$  and  $|b\rangle$  with no momentum transfer. At this stage, modes  $|a, 0\rangle$  and  $|b, k_0\rangle$  each

\*haine@physics.uq.edu.au

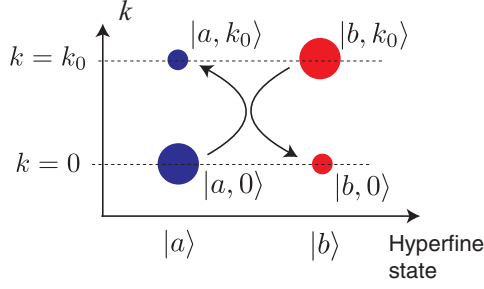


FIG. 1. (Color online) Four-wave mixing.  $s$ -wave collisions between  $|a, 0\rangle$  and  $|b, k_0\rangle$  scatter atoms into  $|a, k_0\rangle$  and  $|b, 0\rangle$ .

contain approximately  $10^5$  atoms, and modes  $|b, 0\rangle$  and  $|a, k_0\rangle$  each contain approximately  $10^3$  atoms, where the notation  $|a(b), k\rangle \equiv |a(b)\rangle|k\rangle$ , and the state  $|k\rangle$  indicates a wave packet traveling with mean momentum  $\hbar k$ .  $s$ -wave collisions between  $|a, 0\rangle$  and  $|b, k_0\rangle$  atoms will transfer particles from  $|a, 0\rangle$  to  $|a, k_0\rangle$ , and  $|b, k_0\rangle$  to  $|b, 0\rangle$ . The creation of one  $|a, k_0\rangle$  atom indicates that a  $|b, 0\rangle$  atom has also been created, as well as the removal of one atom each from modes  $|a, 0\rangle$  and  $|b, k_0\rangle$ . This is the source of the quantum correlations. The 1% seed is optional, as the tight transverse confinement strongly suppresses scattering into other modes. However, we found that the addition of a small seed improved the multimode dynamics of the system, as will be discussed in Sec. IV. After an amount of time  $t_{\text{fwm}}$ , the desired level of four-wave mixing has been achieved, and the two momentum modes completely spatially separate such that, at time  $t_1$ ,  $|a, 0\rangle$  and  $|b, 0\rangle$  are spatially overlapping and centered at locations  $x_L$ , and  $|a, k_0\rangle$  and  $|b, k_0\rangle$  are spatially overlapping and centered at locations  $x_R$ .  $t_{\text{fwm}}$  can be adjusted by adjusting the longitudinal and transverse trapping frequencies, which will adjust the ratio of the characteristic four-wave mixing time and the time taken for the two momentum wave packets to spatially separate. Alternatively, a Feshbach resonance could be used to switch off the  $s$ -wave interactions after an amount of time  $t_{\text{fwm}}$ . At this stage, the system can be thought of as two spin- $\frac{1}{2}$  systems. One, formed by  $|a, 0\rangle$  and  $|b, 0\rangle$  centered at  $x_L$ , and the other formed by  $|a, k_0\rangle$  and  $|b, k_0\rangle$  centered at  $x_R$ .

### III. FOUR-MODE MODEL

In this section we will introduce a simple four-mode model to calculate the degree of quantum correlations generated from the four-wave mixing process. Beginning with a full multimode model describing the system, the Hamiltonian is

$$\mathcal{H} = \sum_j \int \hat{\psi}_j^\dagger(\mathbf{r}) H_0 \hat{\psi}_j(\mathbf{r}) d^3\mathbf{r} + \sum_i \sum_j \frac{U_{ij}}{2} \int \hat{\psi}_i^\dagger(\mathbf{r}) \hat{\psi}_j^\dagger(\mathbf{r}) \hat{\psi}_i(\mathbf{r}) \hat{\psi}_j(\mathbf{r}) d^3\mathbf{r}, \quad (1)$$

where  $j = a, b$ ,  $H_0 = \frac{\hbar^2}{2m} \nabla^2 + V(y, z)$ , and  $U_{ij} \equiv \frac{4\pi\hbar^2 a_{ij}}{m}$ , where  $a_{ij}$  is the inter- and intraspecies scattering length, and  $m$  is the mass of the atom. We can gain insight into the behavior

of the system by introducing a simple four-mode model by making the approximation

$$\hat{\psi}_a(\mathbf{r}) \approx \hat{a}_0 \Psi(x, y, z) + \hat{a}_{k_0} \Psi(x, y, z) e^{ik_0 z}, \quad (2)$$

$$\hat{\psi}_b(\mathbf{r}) \approx \hat{b}_0 \Psi(x, y, z) + \hat{b}_{k_0} \Psi(x, y, z) e^{ik_0 z},$$

where  $\Psi(x, y, z)$  is the (normalized) ground state of the confining potential, before the longitudinal potential was switched off. Substituting this into Eq. (1) gives

$$\mathcal{H} = \sum_{k=0, k_0} \hbar\omega_k (\hat{a}_k^\dagger \hat{a}_k + \hat{b}_k^\dagger \hat{b}_k) + \frac{\hbar\chi}{2} \sum_{k, k'=0, k_0} (\hat{a}_k^\dagger \hat{a}_{k'}^\dagger \hat{a}_k \hat{a}_{k'} + \hat{b}_k^\dagger \hat{b}_{k'}^\dagger \hat{b}_k \hat{b}_{k'} + 2\hat{a}_k^\dagger \hat{a}_{k'} \hat{b}_k^\dagger \hat{b}_{k'}) + \hbar\chi (\hat{a}_{k_0}^\dagger \hat{b}_0^\dagger \hat{a}_0 \hat{b}_{k_0} + \hat{a}_0^\dagger \hat{b}_{k_0}^\dagger \hat{a}_{k_0} \hat{b}_0), \quad (3)$$

where  $\hbar\omega_k = \hbar\omega_0 + \frac{\hbar k^2}{2m}$ , and  $\hbar\omega_0$  is the ground-state eigenvalue of  $H_0$ . The characteristic four-wave mixing rate is  $\chi \equiv U_0 \int |\Psi(x, y, z)|^4 d^3\mathbf{r}$ , and we have assumed that  $U_{aa} = U_{bb} = U_{ab}$ , which is a good approximation for  $^{87}\text{Rb}$ . We have assumed that  $\int |\Psi(x, y, z)|^2 e^{ik_0 x} d^3\mathbf{r} \approx 0$ , which is a good approximation when the momentum spread of the condensate is small  $\hbar k_0$ , or  $k_0 \gg \frac{1}{r_x}$ , where  $r_x$  is the characteristic size of the condensate in the  $x$  direction.

We can gain some insight into the behavior of this system with a simple analytic model. The Heisenberg equations of motion for the two lowly occupied ‘‘seed’’ modes are

$$i\dot{\hat{a}}_{k_0} = (\omega_{k_0} + \chi \hat{N}_t) \hat{a}_{k_0} + \chi \hat{a}_0 \hat{b}_{k_0} \hat{b}_0^\dagger, \quad (4)$$

$$i\dot{\hat{b}}_0 = (\omega_0 + \chi \hat{N}_t) \hat{b}_0 + \chi \hat{a}_0 \hat{b}_{k_0} \hat{a}_{k_0}^\dagger, \quad (5)$$

where  $\hat{N}_t \equiv \hat{a}_0^\dagger \hat{a}_0 + \hat{b}_0^\dagger \hat{b}_0 + \hat{a}_{k_0}^\dagger \hat{a}_{k_0} + \hat{b}_{k_0}^\dagger \hat{b}_{k_0}$  is the total number of atoms, which we will treat as a constant  $\hat{N}_t \rightarrow N_t$  because it is a conserved quantity. We define the number of particles in each mode as  $\hat{N}_{aL} = \hat{a}_0^\dagger \hat{a}_0$ ,  $\hat{N}_{bL} = \hat{b}_0^\dagger \hat{b}_0$ ,  $\hat{N}_{aR} = \hat{a}_{k_0}^\dagger \hat{a}_{k_0}$ , and  $\hat{N}_{bR} = \hat{b}_{k_0}^\dagger \hat{b}_{k_0}$ . Because  $\langle \hat{N}_{aL} \rangle, \langle \hat{N}_{bR} \rangle \gg \langle \hat{N}_{aR} \rangle, \langle \hat{N}_{bL} \rangle$  at  $t = 0$ , we can make the approximation  $\hat{a}_0 \rightarrow \alpha_0$ ,  $\hat{b}_{k_0} \rightarrow \beta_{k_0} e^{-i\omega_{k_0} t}$ , where  $\alpha_0 = (\langle \hat{N}_{aL} \rangle)^{1/2}$ , and  $\beta_{k_0} = (\langle \hat{N}_{bR} \rangle)^{1/2}$ . By ignoring the depletion from these modes, which is acceptable for times  $\chi N_t t \ll 1$ , we find the solution to Eqs. (4) and (5) is

$$\tilde{a}_{k_0}(t) = \hat{a}_{k_0}(0) \cosh r - i\hat{b}_0^\dagger(0) \sinh r, \quad (6)$$

$$\tilde{b}_0(t) = \hat{b}_0(0) \cosh r - i\hat{a}_{k_0}^\dagger(0) \sinh r, \quad (7)$$

with  $r = \chi \alpha_0 \beta_{k_0} t$  and we have made the transformation  $\tilde{a}_{k_0} = \hat{a}_{k_0} e^{i(\omega_{k_0} + N_t \chi) t}$ ,  $\tilde{b}_0 = \hat{b}_0 e^{i(\omega_0 + N_t \chi) t}$ .

The quantity we are interested in is the relative number difference variance, which we define as

$$v_{i,j} \equiv \frac{V(N_-)}{\langle \hat{N}_+ \rangle} = \frac{\langle (\hat{N}_i - \hat{N}_j)^2 \rangle - \langle (\hat{N}_i - \hat{N}_j) \rangle^2}{\langle \hat{N}_i + \hat{N}_j \rangle}. \quad (8)$$

$v_{i,j} = 1$  for two independent Glauber coherent states [27], which is a good approximation of the quantum statistics of a coherently split BEC. Taking the initial quantum state of modes  $|a, k_0\rangle$  and  $|b, 0\rangle$  to be independent Glauber coherent

states with mean populations  $\langle \hat{N}_{aR}(0) \rangle = \langle \hat{N}_{bL}(0) \rangle \equiv N_0$ , we find that

$$\langle \hat{N}_{aR}(t) \rangle = \langle \hat{N}_{bL}(t) \rangle = \left( N_0 + \frac{1}{2} \right) \cosh 2r - \frac{1}{2}, \quad (9)$$

and

$$v_{aR,bL} = \frac{2N_0}{(2N_0 + 1) \cosh 2r - 1}. \quad (10)$$

Figure 2 shows  $\langle \hat{N}_{aR}(t) \rangle$  and  $v_{aR,bL}$  as a function of time.  $v_{aR,bL}$  decreases from 1 exponentially with  $r$ . However, the population grows exponentially, suggesting that our model is invalid for long times, and a model which takes into account depletion is required.

A more complicated analysis of our system which includes effects such as quantum depletion and Kerr dephasing due to uncertainties in the particle number can be achieved by using a stochastic phase-space method. Specifically, we use the truncated Wigner (TW) approach [28], which we will now describe. The master equation for the system is found from Eq. (3) and then converted into a Fokker-Plank equation (FPE) by using the Wigner representation. This equation can then be converted into a set of stochastic differential equations, which we solve numerically. By averaging over many trajectories with different noises in the initial conditions,

expectation values of the quantum field operators can be calculated. When converting our FPE to stochastic differential equations, we ignore terms with third-order derivatives in the FPE, because these terms do not have a simple mapping to the stochastic differential equations and can be assumed to be negligible when the field has high occupation numbers [28]. The stochastic differential equations are

$$i\dot{\alpha}_0 = (\omega_0 + \chi N_t) \alpha_0 + \chi \beta_k^* \beta_0 \alpha_k, \quad (11)$$

$$i\dot{\alpha}_{k_0} = (\omega_{k_0} + \chi N_t) \alpha_k + \chi \beta_0^* \beta_k \alpha_0, \quad (12)$$

$$i\dot{\beta}_0 = (\omega_0 + \chi N_t) \beta_0 + \chi \alpha_k^* \alpha_0 \beta_k, \quad (13)$$

$$i\dot{\beta}_{k_0} = (\omega_{k_0} + \chi N_t) \beta_k + \chi \alpha_0^* \alpha_k \beta_0, \quad (14)$$

where  $N_t = \alpha_0^* \alpha_0 + \alpha_{k_0}^* \alpha_{k_0} + \beta_0^* \beta_0 + \beta_{k_0}^* \beta_{k_0} - 2$  represents the total number of particles. The subtraction of 2 is required due to the correspondence between the complex variables in the stochastic differential equations and symmetrically ordered operators. These complex variables correspond to our original operators:  $\hat{a}_j \rightarrow \alpha_j$ ,  $\hat{a}_j^\dagger \rightarrow \alpha_j^*$ ,  $\hat{b}_j \rightarrow \beta_j$ ,  $\hat{b}_j^\dagger \rightarrow \beta_j^*$ . The noise on the initial conditions for each trajectory of the evolution of these equations was chosen such that they correspond to the quantum statistics of the initial state of interest. Expectation values of symmetrically ordered combinations of field operators correspond to the ensemble average of these complex variables over a large number of trajectories. For example,  $\overline{|\alpha_j|^2} = \frac{1}{2} \langle \hat{a}_j^\dagger \hat{a}_j + \hat{a}_j \hat{a}_j^\dagger \rangle$ , where the overline represents the mean of a large number of trajectories.

We solve our equations of motion choosing our initial conditions as Glauber coherent states for each mode, with  $\langle \hat{N}_{aL}(0) \rangle = \langle \hat{N}_{bR}(0) \rangle = 10^5$  and  $\langle \hat{N}_{aR}(0) \rangle = \langle \hat{N}_{bL}(0) \rangle = 10^3$ . We let the system evolve for an amount of time  $t_{\text{fwm}}$ . In practice,  $t_{\text{fwm}}$  is determined by the separation time for the two momentum components, and can be adjusted by manipulation of the longitudinal trapping frequency. Alternatively,  $\chi$  can be adjusted by manipulation of the scattering length via a Feshbach resonance, or by adjusting the transverse trapping frequency. Figure 2 shows the populations of each mode as a function of  $t_{\text{fwm}}$ . The four-wave mixing creates correlations in particle number between modes  $|a, k_0\rangle$  and  $|b, 0\rangle$ , which we quantify by examining the normalized number difference variance  $v_{aR,bL}$ . As  $t_{\text{fwm}}$  increases,  $v_{aR,bL}$  initially decreases exponentially until the effects of quantum depletion limit the amount of squeezing. A minimum value of  $v_{aR,bL} \approx 10^{-2}$  is reached at  $N_t \chi t_{\text{fwm}} \approx 10$ , before the correlations begin to decrease again. All other binary combinations of modes display anticorrelations as a result of the four-wave mixing. The degree by which these quantum correlations can enhance an interferometric measurement are show in Fig. 5.

#### IV. MULTIMODE EFFECTS

To investigate the validity of the approximations we made in the previous section, we introduce a one-dimensional model to investigate the effect of multimode dynamics on the four-wave mixing process. Assuming the dynamics in the  $y$  and  $z$  dimensions is trivial, we reduce Eq. (1) to one dimension by integrating over the  $y$  and  $z$  dimensions. We then derive a set of stochastic partial differential equations for the complex

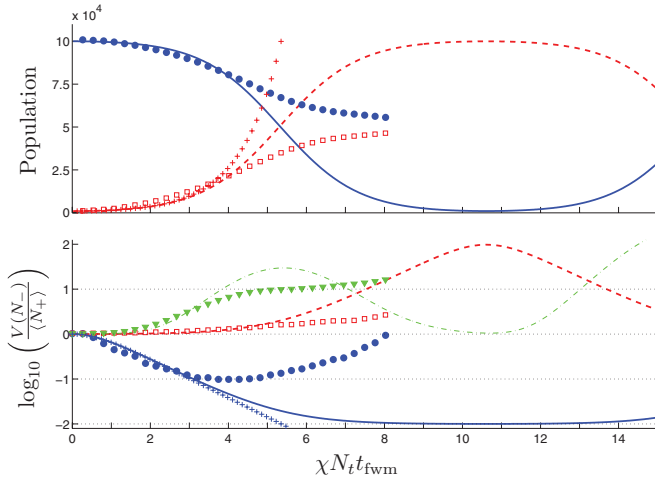


FIG. 2. (Color online) (a) Populations of each mode as a function of  $t_{\text{fwm}}$ .  $\langle \hat{N}_{aL} \rangle$  was calculated using the four-mode TW model (blue solid line), and the one-dimensional (1D) multimode TW model (blue solid circles).  $\langle \hat{N}_{bL} \rangle$  was calculated using a simple model with no depletion (red “+” symbols), the four-mode TW model (red dashed line), and the 1D multimode TW model (red squares).  $\langle \hat{N}_{aR} \rangle$  and  $\langle \hat{N}_{bR} \rangle$  were omitted, because they are almost identical to  $\langle \hat{N}_{bL} \rangle$  and  $\langle \hat{N}_{aL} \rangle$ , respectively. (b) Normalized number difference variance  $v_{i,j}$  for  $\{i,j\} = \{aR,bL\}$  (blue “+” symbols show simple mode with no depletion, blue solid line shows four-mode TW model, blue solid circles show 1D multimode TW model),  $\{aL,bR\}$  (red dashed line shows four-mode TW model, red squares show 1D multimode TW model), and  $\{aL,bL\}$  (green dot-dashed line shows four-mode TW model, green triangles shows 1D multimode TW model).  $\{aR,bR\}$ ,  $\{aL,aR\}$ , and  $\{bL,bR\}$  are omitted because they are almost identical to  $\{aL,bL\}$ . The multimode calculation agrees well with the four-mode calculation for small values of  $t_{\text{fwm}}$ , but does not reach the same degree of squeezing.

functions  $\psi_i(x)$  corresponding to the quantum operator  $\hat{\psi}_i(x)$  via the same method as described in the previous section [18]:

$$i\hbar \frac{d}{dt} \psi_a = \left( \frac{-\hbar^2}{2m} \frac{\partial^2}{\partial x^2} + U_{1d} n_t(x) \right) \psi_a(x), \quad (15)$$

$$i\hbar \frac{d}{dt} \psi_b = \left( \frac{-\hbar^2}{2m} \frac{\partial^2}{\partial x^2} + U_{1d} n_t(x) \right) \psi_b(x), \quad (16)$$

where  $n_t(x) = (|\psi_a(x)|^2 - \frac{1}{2\Delta x}) + (|\psi_b(x)|^2 - \frac{1}{2\Delta x})$  is the total density, where  $\Delta x$  is the grid spacing. The subtraction of  $\frac{1}{2\Delta x}$  is to compensate for the mean field of the vacuum, which is nonzero in the truncated Wigner approach.  $U_{1d} = \frac{U_0}{\pi r_0^2}$  is the one-dimensional interaction strength, and  $r_0$  is the characteristic transverse width of the condensate. The initial condition is chosen to be analogous to the initial condition in the four-mode model:

$$\begin{aligned} \psi_a(x,0) &= \sqrt{10^5} \Psi_0(x) + \sqrt{10^3} \Psi_0(x) e^{ik_0 x} + \frac{\eta_1(x)}{\sqrt{\Delta x}}, \\ \psi_b(x,0) &= \sqrt{10^3} \Psi_0(x) + \sqrt{10^5} \Psi_0(x) e^{ik_0 x} + \frac{\eta_2(x)}{\sqrt{\Delta x}}, \end{aligned}$$

where  $\eta_j(x)$  are complex Gaussian noise functions with standard deviation in the real and imaginary components of one half and  $\langle \eta_n^*(x_i) \eta_m(x_j) \rangle = \frac{1}{2} \delta_{i,j} \delta_{n,m}$ . In the TW method, the expectation value of the density of state- $|j\rangle$  atoms is  $\langle \hat{\psi}_j^\dagger(x) \hat{\psi}_j(x) \rangle = |\psi_j(x)|^2 - \frac{1}{2\Delta x}$ . At  $t = 0$ , confinement in the  $x$  direction is switched off, whilst keeping the transverse confining potential, and the two wave packets are allowed to spatially separate. After an amount of time  $t_{\text{fwm}}$ , the  $s$ -wave scattering length is switched to zero using a Feshbach resonance, to control the amount of four-wave mixing that will occur. After 70 ms, the wave packets have completely separated, and we measure the number of atoms on either side of a central position  $x_0$ . Using this measurement, we can define the quantities analogous to the populations of the four modes in the previous section as

$$\hat{N}_{aL} \equiv \int_{-\infty}^{x_0} \hat{\psi}_a^\dagger(x) \hat{\psi}_a(x) dx, \quad (17)$$

$$\hat{N}_{bL} \equiv \int_{-\infty}^{x_0} \hat{\psi}_b^\dagger(x) \hat{\psi}_b(x) dx, \quad (18)$$

$$\hat{N}_{aR} \equiv \int_{x_0}^{\infty} \hat{\psi}_a^\dagger(x) \hat{\psi}_a(x) dx, \quad (19)$$

$$\hat{N}_{bR} \equiv \int_{x_0}^{\infty} \hat{\psi}_b^\dagger(x) \hat{\psi}_b(x) dx. \quad (20)$$

Figure 2(a) shows the populations in each of these modes as a function of  $t_{\text{fwm}}$ . For early times  $N_t \chi t_{\text{fwm}} \lesssim 4$  ( $t_{\text{fwm}} \lesssim 150 \mu\text{s}$ ), the multimode model mimics the simple four-mode model. This is also the time when the variances [Fig. 2(b)] begin to deviate from the simple four-mode model and  $v_{aL,bR}$  reaches its minimum value  $v_{aL,bR} \approx 0.1$ , almost a factor of ten away from the minimum predicted from the simple four-mode model. The discrepancy is due to complications arising from multimode effects. Figure 3 shows the expectation value of the density of the atomic clouds after separation for  $t_{\text{fwm}} = 0.1$  ms ( $N_t \chi t_{\text{fwm}} \approx 2.68$ ) and  $t_{\text{fwm}} = 0.18$  ms ( $N_t \chi t_{\text{fwm}} \approx 4.82$ ). In Fig. 3(a), the density profile of all wave packets closely

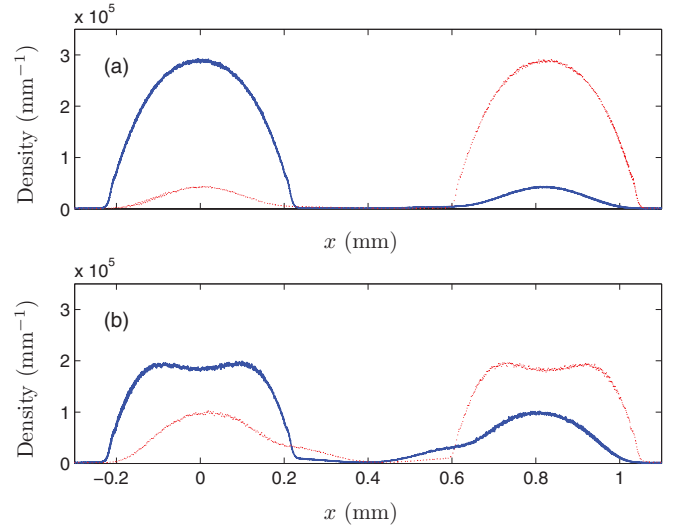


FIG. 3. (Color online)  $\langle \hat{\psi}_a^\dagger(x) \hat{\psi}_a(x) \rangle$  (blue solid line) and  $\langle \hat{\psi}_b^\dagger(x) \hat{\psi}_b(x) \rangle$  (red dotted line) after 70 ms of separation time for (a)  $t_{\text{fwm}} = 0.1$  ms and (b)  $t_{\text{fwm}} = 0.18$  ms. The expectation values were calculated from 1200 trajectories. The trapping frequencies of the harmonic potential at  $t = 0$  were  $\{\omega_x, \omega_y, \omega_z\} = 2\pi \{5, 1000, 1000\}$  Hz. The interaction strength was scaled by the cross-sectional area of the condensate:  $U_{1d} = \frac{U}{\pi r_0^2}$  with  $r_0 = 0.55 \mu\text{m}$ .  $x_0$  was chosen as the point  $x = 0.4$  mm, which is roughly halfway between the two wave packets.

resembles that of the initial state, suggesting that Eq. (2) is a good approximation in this case. However, Fig. 3(b) shows significant deviation from these spatial modes. One cause of this is that the density is higher in the center of each cloud, so the four-wave mixing occurs at a greater rate there, increasing the depletion. It is interesting to note that discrepancies begin to arise in all three models at roughly the same point, as the quantum depletion which causes the undepleted pump model to break down also causes the approximation in Eq. (2) to break down, as the depletion alters the shape of the spatial mode. The second effect is the finite momentum spread of the wave packet and allows for spontaneous scattering to unpopulated momentum modes, which slowly grow. This is the cause of the “tails” leading out from the condensate in Fig. 3(b). Without the 1% “seed” in the lowly occupied modes, we observe a greater degree of this spontaneous scattering. However, increasing the initial population in the seed modes degrades the degree of quantum correlations. Picking the optimum level of initial population in these modes is a trade-off between suppressing spontaneous scattering into unpopulated modes, and degrading the degree of quantum correlations produced. We did not do a comprehensive search to find the optimum value of this initial population, but found that the model behaved to our satisfaction with a 1% seed. This effect of spontaneous scattering is not present in a semiclassical model, because spontaneous scattering is forbidden.

## V. INTERFEROMETRY BELOW THE STANDARD QUANTUM LIMIT

The obvious method for using the state generated from the four-wave mixing process to perform phase measurements

with sensitivity greater than the standard quantum limit would be to use  $|a, k_0\rangle$  and  $|b, 0\rangle$  as the inputs to an atom interferometer, as these are the modes which display two-mode squeezing. However, there are two drawbacks to this approach: The first is that each of these modes are only lowly occupied so, although they would display subshotnoise sensitivity when used in the appropriate way for an interferometric measurement, the absolute sensitivity of the measurement would be low, because the total number of particles is small. The second drawback is that these modes are not spatially overlapping, so a complicated sequence of momentum-shaping pulses would be required in order to construct an atom interferometer out of these two wave packets. By combining these two lowly occupied modes with  $|a, 0\rangle$  and  $|b, k_0\rangle$ , which have a much higher occupation, we may be able to maintain the advantage of the quantum squeezing, while increasing the total number of particles, such that the absolute sensitivity is increased. Additionally,  $|a, 0\rangle$  and  $|b, 0\rangle$  form a spatially overlapping pair, as do  $|a, k_0\rangle$  and  $|b, k_0\rangle$ . We can combine these four modes to make an interferometric measurement in the following way: The interferometry stage is implemented by a sequence of  $\frac{\pi}{2}$  microwave pulses resonant with the  $|a\rangle \rightarrow |b\rangle$  transition, which provides local coupling for the spatially overlapping wave packets. Our scheme is described in Fig. 4. In total, three coupling pulses are used, with a phase shift on  $|b, 0\rangle$  and  $|b, k_0\rangle$  before each coupling pulse. Phase shifts on the left and right wave packet need to be controlled independently. This could be implemented by the ac Stark shift from independent focused optical beams. The first coupling pulse is used to prepare the state such that it is useful for atom interferometry, with the phase shift before the first pulse chosen such that

the populations in  $|a, 0\rangle$  and  $|b, 0\rangle$ , and  $|a, k_0\rangle$  and  $|b, k_0\rangle$  are approximately equal after the first beam splitter. At this stage, the quantity  $\hat{S} \equiv (\hat{N}_{aL} - \hat{N}_{bL}) - (\hat{N}_{bR} - \hat{N}_{aR})$  is squeezed. That is, the variance in this quantity is much less than for uncorrelated sources. The phase shift before the second coupling pulse is again chosen such that the populations remain equal. At this point,  $\hat{S}$  is antisqueezed, and the relative phase will be squeezed. The physical process of interest causes a phase shift  $\phi_{2L}$  between  $|a, 0\rangle$  and  $|b, 0\rangle$  and  $\phi_{2R}$  between  $|a, k_0\rangle$  and  $|b, k_0\rangle$  to be accumulated during the free evolution between the second and third coupling pulses. After the third coupling pulse, the the number of atoms in each mode is measured, and  $S$  is calculated.

For any interferometric device, the smallest detectable phase shift is

$$\Delta\phi = \frac{\sqrt{V(S)}}{\left|\frac{d\langle\hat{S}\rangle}{d\phi}\right|}, \quad (21)$$

where  $S$  is the measured signal. The ultimate limit for sensitivity is the Heisenberg limit  $\Delta\phi = \frac{1}{N_t}$ , where  $N_t$  is the total number of detected atoms. However, when using uncorrelated atoms as the input to the interferometer, the maximum sensitivity is given by the standard quantum limit,  $\Delta\phi = \frac{1}{\sqrt{N_t}}$  [10].

After the wave packets have spatially separated, we essentially have two interferometers; one centered at  $x_L$ , and the other centered at  $x_R$ . When treating our two interferometers separately, the sensitivity of each device is well above the standard quantum limit. However, when taking our signal to be the difference in the two signals,  $\hat{S} = (\hat{N}_{aL} - \hat{N}_{bL}) - (\hat{N}_{bR} - \hat{N}_{aR})$ , it may be possible to observe an enhancement in sensitivity, because we have correlations between the left and right systems. We will consider the case where the same applied phase  $\phi_2$  is applied to the left and right interferometers, with a constant offset of  $\pi$  added to the right interferometer (i.e.,  $\phi_{2L} = \phi_2$ ,  $\phi_{2R} = \pi + \phi_2$ ). In this configuration, the system is set up to measure some quantity that effects each interferometer equally, such as a homogeneous magnetic field. By removing the phase shift  $\pi$  from the right interferometer, the system is now configured to measure the *difference* in the external phase shifts and is suited to measure some quantity which is different for each interferometer, such as detecting the difference in magnetic field at two points. Figure 5 shows  $\langle\hat{S}\rangle$ ,  $\frac{V(S)}{\langle N_t \rangle}$ , and  $\Delta\phi$  as a function of  $\phi_2$  after the third coupling pulse for  $t_{\text{fwm}} = 0.12$  ms. The minimum of  $\Delta\phi\sqrt{N_t}$  for the multimode model is  $\Delta\phi\sqrt{N_t} \approx 0.41$ , which is more than twice as sensitive than for uncorrelated atoms. The fringe visibility of the final interferometric measurement is  $\sim 0.999$  for the four-mode model, and  $\sim 0.935$  for the multimode model.

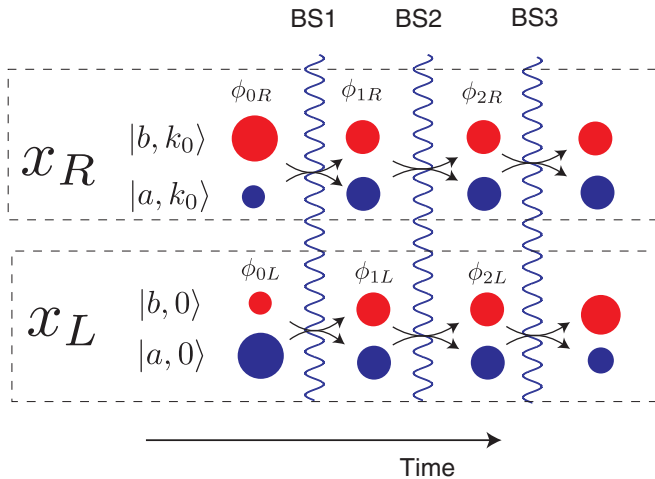


FIG. 4. (Color online) Pulse sequence. After the two momentum modes have spatially separated, the interferometry stage is implemented by a sequence of three  $\frac{\pi}{2}$  pulses. An appropriate phase shift  $\phi_{0L}$  is applied to  $|b, 0\rangle$  and  $\phi_{0R}$  to  $|b, k_0\rangle$  before the first coupling pulse and  $\phi_{1L}$  and  $\phi_{1R}$  before the second pulse to ensure that the populations in each mode remain approximately equal after each pulse. These phase shifts may be different, and can be implemented using the ac Stark shift from a localized optical beam. The phase shifts  $\phi_{2L}$  and  $\phi_{2R}$  between the second and third pulses is the quantity that the interferometer measures. The population in each mode is measured after the third beam splitter.

## VI. COMPARISON WITH ONE-AXIS TWISTING

An alternate scheme for performing atom interferometry with subshotnoise sensitivity is the previously discussed one-axis twisting scheme [11–14]. This scheme involves splitting the condensate and allowing the nonlinear interactions to “shear” the relative phase of the two modes until the desired level of spin squeezing is reached. However, at this point, the squeezing is not directly usable, and the quadrature squeezing

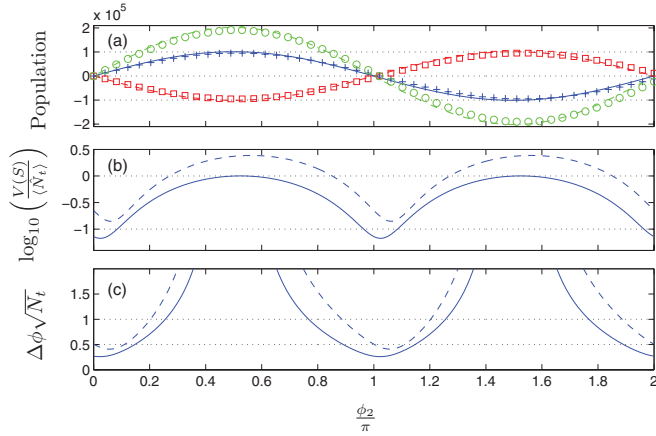


FIG. 5. (Color online) (a)  $\langle \hat{N}_{aL} - \hat{N}_{bL} \rangle$  (blue solid line shows four-mode TW model, blue “+” symbols show 1D multimode TW model),  $\langle \hat{N}_{bR} - \hat{N}_{aR} \rangle$  (red dashed line shows four-mode TW model and red squares show 1D multimode TW model), and  $\langle \hat{S} \rangle$  (green dot-dashed line shows four-mode TW model and green circles show 1D multimode TW model) as a function of  $\phi_2$ . The four-mode model has slightly more fringe visibility than the 1D multimode model. The horizontal black dotted lines are a visual guide only. (b)  $\frac{V(S)}{\langle \hat{N}_t \rangle}$  from the four-mode model (solid blue line), and the multimode model (dashed blue line) as a function of  $\phi_2$ . The horizontal black dotted lines indicated the level expected for uncorrelated atoms [ $\log_{10}(V(S)/\langle \hat{N}_t \rangle) = 0$ ], and squeezing below the uncorrelated level by a factor of 10 [ $\log_{10}(V(S)/\langle \hat{N}_t \rangle) = -1$ ]. (c) The phase sensitivity  $\Delta\phi$  from the four-mode model (blue solid line) and multimode model (blue dashed line). The minimum of  $\Delta\phi\sqrt{N_t}$  for the multimode model is  $\Delta\phi \approx 0.41\sqrt{N_t}$ —more than twice as sensitive than for uncorrelated atoms.

needs to be rotated by an angle  $\theta$  such that there are reduced fluctuations in the relative phase. In order to achieve this, an additional phase shift and a coupling pulse is applied in a method analogous to that discussed in Sec. V of this article. Significant antisqueezing instead of squeezing will be observed if the incorrect phase shift is applied. This phase shift depends critically on the total number of particles, because the nonlinear effect which causes the phase shearing also causes a relative phase shift between the two modes which depends on the number of particles. As the number of particles becomes large, a small variation in the total number of particles is sufficient to significantly alter the relative phase of the two modes and thus to rotate the squeezing quadrature such that antisqueezing is observed.

To compare the performance of the one-axis twisting scheme to our four-wave mixing scheme, we analyzed the one-axis twisting scheme via the two-mode model described in [14]. To demonstrate subshotnoise sensitivity, one would have to find the optimum value of the phase shift and then perform many shots of the experiment to build up quantum statistics in

the signal. We set the total number of particles as  $2 \times 10^5$ , and optimizing the nonlinear interaction time, coupling pulses, and phase shifts, such that the phase sensitivity of the device was  $\Delta\phi\sqrt{N_t} \approx 0.4$ . We then varied the total number by a small amount, whilst keeping all other parameters (phase shifts and coupling pulses) fixed. We found that altering the total number of particles by about 1% was enough to decrease the sensitivity to the limit set by shotnoise ( $\Delta\phi = \frac{1}{\sqrt{N_t}}$ ). It is important to note that this degradation of the signal is not due simply to the fluctuations in the number of atoms directly adding noise to the signal, because the signal (i.e., difference in the number of atoms in each mode) is insensitive to fluctuations in the total number of atoms. A small shift in total number causes a big shift to the value of the phase shift required in order to rotate the squeezing to the correct quadrature. However, when the total number of atoms was small ( $\sim 1000$ ), as in the recent experiments by [11,12], a small fluctuation in total number causes a relatively small phase shift, and a perturbation in the number of particles of  $\sim 35\%$  was required in order to decrease the sensitivity to the shotnoise limit.

As the Hamiltonian for the four-wave mixing process does not rely on asymmetric scattering lengths between the two modes, the process that produces the correlation does not also cause a number-dependent phase shift. We found that altering the initial number by 50% in a simple four-mode calculation, while keeping all other parameters the same as used in Figure 5 ( $\chi$ ,  $t_{\text{fwm}}$ ,  $\phi_{0R}$ ,  $\phi_{1R}$ ,  $\phi_{2R}$ ,  $\phi_{0L}$ ,  $\phi_{1L}$ , and  $\phi_{2L}$ ), the shotnoise limit was still surpassed. This indicates that four-wave mixing is sufficiently robust against shot-to-shot number fluctuations that it can be used with a large number of particles.

## VII. CONCLUSION

We have demonstrated that quantum correlations generated from four-wave mixing can be utilized to perform atom interferometry with sensitivity greater than the standard quantum limit. Over longer timescales, multimode effects cause complicated evolution in the spatial mode of the wave packets, which reduce the strength of the useful correlations and ultimately limit the amount of squeezing one can produce. By combining lowly occupied yet correlated modes with the two remaining highly occupied modes, it is possible to surpass the shotnoise limit, while still using a large number of atoms, increasing the absolute sensitivity of the device.

## ACKNOWLEDGMENTS

We would like to acknowledge useful discussions with Matthew Davis, Tod Wright, and Jacopo Sabatini. This work was supported by the Australian Research Council Centre of Excellence for Quantum-Atom Optics and by Australian Research Council discovery project DP0986893.

- [1] Alexander D. Cronin, Jörg Schmiedmayer, and David E. Pritchard, *Rev. Mod. Phys.* **81**, 1051 (2009).  
 [2] A. Peters, K. Y. Chung, and S. Chu, *Nature (London)* **400**, 849 (1999).

- [3] A. Peters, K. Y. Chung, and S. Chu, *Meterologia* **38**, 25 (2001).  
 [4] J. M. McGuirk, G. T. Foster, J. B. Fixler, M. J. Snadden, and M. A. Kasevich, *Phys. Rev. A* **65**, 033608 (2002).

- [5] T. L. Gustavson, P. Bouyer, and M. A. Kasevich, *Phys. Rev. Lett.* **78**, 2046 (1997).
- [6] M. Vengalattore, J. M. Higbie, S. R. Leslie, J. Guzman, L. E. Sadler, and D. M. Stamper-Kurn, *Phys. Rev. Lett.* **98**, 200801 (2007).
- [7] J. B. Fixler, G. T. Foster, J. M. McGuirk, and M. A. Kasevich, *Science* **315**, 5808 (2007).
- [8] R. Bouchendira, P. Clade, S. Guellati-Khelifa, F. Nez, and F. Biraben, *Phys. Rev. Lett.* **106**, 080801 (2011).
- [9] J. E. Debs, P. A. Altin, T. H. Barter, D. Döring, G. R. Dennis, G. McDonald, R. P. Anderson, J. D. Close, and N. P. Robins, *Phys. Rev. A* **84**, 033610 (2011).
- [10] J. P. Dowling, *Phys. Rev. A* **57**, 4736 (1998).
- [11] C. Gross, T. Zibold, E. Nicklas, J. Esteve, and M. K. Oberthaler, *Nature (London)* **464**, 1165 (2010).
- [12] M. F. Riedel, P. Bohl, Y. Li, T. W. Hansch, A. Sinatra, and P. Treutlein, *Nature (London)* **464**, 1170 (2010).
- [13] M. Kitagawa and M. Ueda, *Phys. Rev. A* **47**, 5138 (1993).
- [14] S. A. Haine and M. T. Johnsson, *Phys. Rev. A* **80**, 023611 (2009).
- [15] L. Deng, E. W. Hagley, J. Wen, M. Trippenbach, Y. Band, P. S. Julienne, J. Simsarian, K. Helmerson, S. L. Rolston, and W. D. Phillips, *Nature (London)* **398**, 218 (1999).
- [16] J. M. Vogels, K. Xu, and W. Ketterle, *Phys. Rev. Lett.* **89**, 020401 (2002).
- [17] J. M. Vogels, J. K. Chin, and W. Ketterle, *Phys. Rev. Lett.* **90**, 030403 (2003).
- [18] A. J. Ferris, M. K. Olsen, and M. J. Davis, *Phys. Rev. A* **79**, 043634 (2009).
- [19] P. Zin, J. Chwedenczuk, A. Veitia, K. Rzkazewski, and M. Trippenbach, *Phys. Rev. Lett.* **94**, 200401 (2005).
- [20] P. Deuar and P. D. Drummond, *Phys. Rev. Lett.* **98**, 120402 (2007).
- [21] M. Ögren and K. V. Kheruntsyan, *Phys. Rev. A* **79**, 021606 (2009).
- [22] R. G. Dall, L. J. Byron, A. G. Truscott, G. R. Dennis, M. T. Johnsson, and J. J. Hope, *Phys. Rev. A* **79**, 011601 (2009).
- [23] G. R. Dennis and M. T. Johnsson, *Phys. Rev. A* **82**, 033615 (2010).
- [24] A. Perrin, H. Chang, V. Krachmalnicoff, M. Schellekens, D. Boiron, A. Aspect, and C. I. Westbrook, *Phys. Rev. Lett.* **99**, 150405 (2007).
- [25] J. C. Jaskula, M. Bonneau, G. B. Partridge, V. Krachmalnicoff, P. Deuar, K. V. Kheruntsyan, A. Aspect, D. Boiron, and C. I. Westbrook, *Phys. Rev. Lett.* **105**, 190402 (2010).
- [26] D. Pertot, B. Gadway, and D. Schneble, *Phys. Rev. Lett.* **104**, 200402 (2010).
- [27] D. F. Walls and G. J. Milburn, *Quantum Optics* (Springer, Berlin, 1994).
- [28] A. A. Norrie, R. J. Ballagh, and C. W. Gardiner, *Phys. Rev. A* **73**, 043617 (2006).